Scattering of Sound from Point Sources by Multiple Circular Cylinders Using Addition Theorem and Superposition Technique

AQ2

Jeng-Tzong Chen,[1,2] **Ying-Te Lee,**[1] **Yi-Jhou Lin,**[1] **I-Lin Chen,**[3] **Jia-Wei Lee**[1]

[1] *Department of Harbor and River Engineering, National Taiwan Ocean University, Keelung 20224, Taiwan*

[2] *Department of Mechanical and Mechatronics Engineering, National Taiwan Ocean University, Keelung 20224, Taiwan*

[3] *Department of Naval Architecture, National Kaohsiung Marine University, Kaohsiung 81157, Taiwan*

Received 4 February 2009; accepted 21 January 2010
Published online in Wiley InterScience (www.interscience.wiley.com).
DOI 10.1002/num.20583

In this study, we use the addition theorem and superposition technique to solve the scattering problem with multiple circular cylinders arising from point sound sources. Using the superposition technique, the problem can be decomposed into two individual parts. One is the free-space fundamental solution. The other is a typical boundary value problem (BVP) with specified boundary conditions derived from the addition theorem by translating the fundamental solution. Following the success of null-field boundary integral formulation to solve the typical BVP of the Helmholtz equation with Fourier densities, the second-part solution is easily obtained after collocating the observation point exactly on the real boundary and matching the boundary condition. The total solution is obtained by superimposing the two parts which are the fundamental solution and the semianalytical solution of the Helmholtz problem. An example was demonstrated to validate the present approach. The parameter study of size and spacing between cylinders are addressed. The results are well compared with the available theoretical solutions and experimental data.
Numer Methods Partial Differential Eq 000: 000–000, 2010

Keywords: addition theorem; Fourier series; null-field integral formulation; scattering; superposition technique

I. INTRODUCTION

Multiple scattering problems occur in many applications related to various areas of applied science, e.g., acoustics [1,2], electromagnetism [3,4], elasticity [5], and water-wave [6] problems. Mathematically speaking, the scattering field appears as the superposition of free field and radiation field.

Correspondence to: Jeng-Tzong Chen, Department of Harbor and River Engineering, National Taiwan Ocean University, Keelung 20224, Taiwan (e-mail: jtchen@mail.ntou.edu.tw)

A better understanding of scattering phenomenon requires a precise knowledge of the influence of the different geometrical and physical parameters of the problem. Owing to the complexity of this problem, a numerical solution is always resorted, especially in the case where the number, radii, and positions of objects are arbitrary. It can be consulted with the textbook of Martin [7].

Many researchers investigated the point source problems in the past years. Row [3, 8] successfully measured the experimental data of the interaction between two circular cylinders within an infinite domain. When the point source is far away the scatter, the problem can be seen as a multiple scattering problem subject to the plane wave. Sherer [1] developed an analytical method for solving the scattering problem with multiple, rigid circular cylinders arranged in an arbitrary configuration. He used the Hankel transform method to calculate the incident field and determined the scattering fields from each cylinder in the collection through the separation of variables. The scattering problem from an array of circular cylinders with oblique incidence plane wave is investigated by Henin et al. [4]. Not only transverse magnetic (TM) but also transverse electric (TE) incident plane waves were considered. Interaction between two penetrable cylinders subject to the oblique incidence were studied by Yousif and Köhler [9]. Some special cases of normal incidence, small radii, perfectly conducting cylinders, and a single cylinder are also considered.

Recently, Chen et al. [10–13] developed the null-field integral equation in conjunction with the degenerate kernel to solve many engineering problems. They claimed that their approaches is one kind of semianalytical approaches as the error comes from truncating the terms of Fourier series. However, the ill-conditioned problem is arisen when the null-field integral equations are used. This is why people prefer collocation on boundary even though there are some singularity issues to solve. Li proposed two other kinds of semianalytical approaches, one can combine with FEM and FDM, and the other use the method of fundamental solutions as given in the Li's book [14] and paper [15], respectively. Nonsingular formulation of the Trefftz method was studied by Li et al. [16]. If the boundary element method (BEM) is used, Cauchy principal value or finite part concept is required to calculate the singular or hypersingular inteqrals [17]. An idea using the null-field integral formulation but collocating on the real boundary without singularity is proposed by Chen et al. [10–13]. Five advantages, mesh-free generation, well-posed model, free of calculating principal value (the singular or hypersingular integrals are transformed into series summability by introducing degenerate kernels and Fourier series), elimination of boundary-layer effect, and exponential convergence, are obtained. They also extended their approach to derive the antiplane dynamic Green's function [18]. Not only perfect but also imperfect interface problems were addressed. Chen et al. [19] have also proposed a logical approach to construct the Green's function of Laplace operator by using the addition theorem and the superposition technique. The null-field integral formulation has been successfully used to solve the Laplace [10, 20], Helmholtz [12, 13], biharmonic [21], and bi-Helmholtz [22] problems.

In this study, the addition theorem and superposition technique are used to solve the scattering problem with multiple circular cylinders arising from point sound sources. The problem is decomposed into two parts. One is the problem of the fundamental solution for the free field. The other is a typical Boundary Value Problem (BVP) with specified boundary conditions derived from the addition theorem by translating the fundamental solution. Following the success of null-field boundary integral formulation in conjunction with degenerate kernel to solve the typical BVP, the second part solution can be easily obtained after collocating the observation point exactly on the real boundary and matching boundary condition. The total solution is obtained by superimposing the two parts. An example was demonstrated to validate the proposed approach. The parameters of size and spacing of cylinders are considered. The results are compared well with the available theoretical solutions and experimental data.

 AQ1

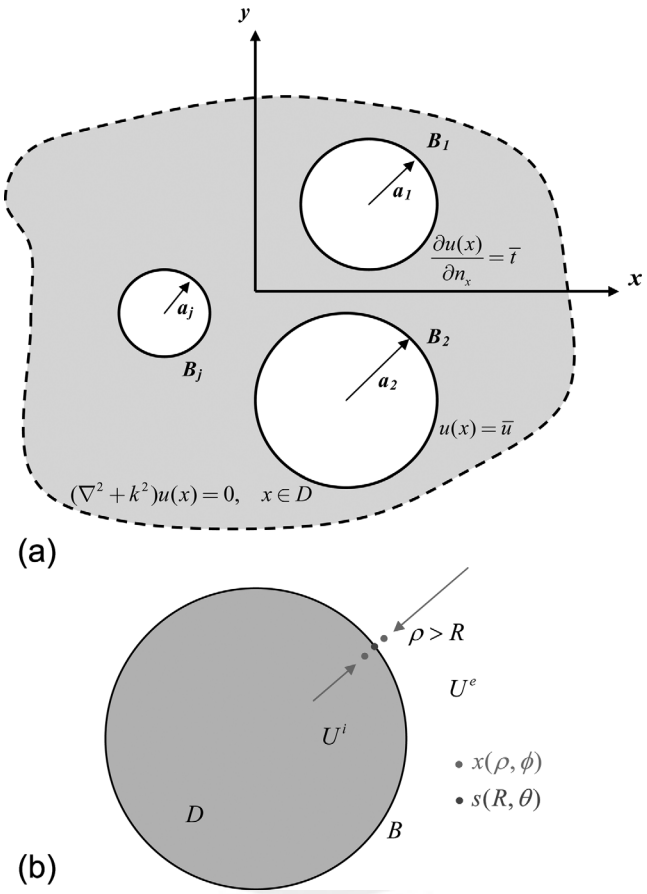

FIG. 1. (a) An infinite plane with arbitrary number of circular cylinders subject to the Dirichlet or Neumann boundary conditions. (b) A simple figure for explaining the degenerate kernels in the interior problem. [Color figure can be viewed in the online issue, which is available at www.interscience.wiley.com.] AQ3

II. NULL-FIELD INTEGRAL FORMULATION FOR A TYPICAL BVP

A. Problem Statements for BVP Without Sources

A typical BVP with H randomly distributed circular cylinders bounded in an infinite domain enclosed with the boundaries, $B_j (j = 1, 2, \ldots, H)$ as shown in Fig. 1(a), F1

$$B = \bigcup_{j=1}^{H} B_j, \tag{1}$$

is considered here. The field $u(x)$ satisfies

$$(\nabla^2 + k^2)u(x) = 0, \quad x \in D, \tag{2}$$

where D is the domain, ∇^2 is the Laplacian operator, k is the wave number which is the angular frequency over the speed of sound. The boundary condition can be specified to either Dirichlet or Neumann type as follows:

$$u(x) = \bar{u}, \quad x \in B, \quad \text{or} \quad \frac{\partial u(x)}{\partial n_x} = \bar{t}, \quad x \in B. \tag{3}$$

The radiation condition is shown below:

$$\frac{\partial u(x)}{\partial n_x} - iku(x) = 0, \quad x \in B_\infty, \tag{4}$$

where B_∞ is the virtual boundary at infinity. This problem is a typical BVP and can be easily solved by using the null-field integral approach.

B. Dual Null-Field Integral Formulation: The Conventional Version

On the basis of the dual integral formulation [10] for the domain point, we have

$$2\pi u(x) = \int_B T(s,x)u(s)dB(s) - \int_B U(s,x)\frac{\partial u(s)}{\partial n_s}dB(s), \quad x \in D, \tag{5}$$

$$2\pi \frac{\partial u(x)}{\partial n_x} = \int_B M(s,x)u(s)dB(s) - \int_B L(s,x)\frac{\partial u(s)}{\partial n_s}dB(s), \quad x \in D, \tag{6}$$

where s and x are the source and field points, respectively. B is the boundary, n_x and n_s denote the outward normal vector at field point and source point, respectively, and the kernel function $U(s,x)$ is the fundamental solution which satisfies

$$(\nabla^2 + k^2)U(x,s) = 2\pi\delta(x-s), \tag{7}$$

where $\delta(x-s)$ denotes the Dirac-delta function. The other kernel functions can be obtained as

$$T(s,x) = \frac{\partial U(s,x)}{\partial n_s}, \tag{8}$$

$$L(s,x) = \frac{\partial U(s,x)}{\partial n_x}, \tag{9}$$

$$M(s,x) = \frac{\partial^2 U(s,x)}{\partial n_s \partial n_x}. \tag{10}$$

By moving the field point x to the boundary, the dual boundary integral equations can be obtained as follows:

$$\pi u(x) = \text{CPV}\int_B T(s,x)u(s)dB(s) - \text{RPV}\int_B U(s,x)\frac{\partial u(s)}{\partial n_s}dB(s), \quad x \in B, \tag{11}$$

$$\pi \frac{\partial u(x)}{\partial n_x} = \text{HPV}\int_B M(s,x)u(s)dB(s) - \text{CPV}\int_B L(s,x)\frac{\partial u(s)}{\partial n_s}dB(s), \quad x \in B, \tag{12}$$

where RPV is the Riemann principal value, CPV is the Cauchy principal value, and HPV is the Hadamard (or called Mangler) principal value. By moving the field point to the complementary domain, the dual null-field integral equations are shown as follows:

$$0 = \int_B T(s,x)u(s)dB(s) - \int_B U(s,x)\frac{\partial u(s)}{\partial n_s}dB(s), \quad x \in D^c, \tag{13}$$

$$0 = \int_B M(s,x)u(s)dB(s) - \int_B L(s,x)\frac{\partial u(s)}{\partial n_s}dB(s), \quad x \in D^c, \tag{14}$$

where "D^c" denotes the domain outside D.

C. Dual Null-Field Integral Formulation: The Present Version

Following the success of null-field integral formulation for the Laplace problem [10], we extend to the Helmholtz case here. By introducing the degenerate kernel, the collocation point can be exactly located on the real boundary free of calculating singular integrals in the sense of principal value. Therefore, the integral equations for the domain point and null-field integral equations in the interior problem are represented as follows:

$$2\pi u(x) = \int_B T^{\mathrm{i}}(s,x)u(s)dB(s) - \int_B U^{\mathrm{i}}(s,x)\frac{\partial u(s)}{\partial n_s}dB(s), \quad x \in D \cup B, \tag{15}$$

$$2\pi \frac{\partial u(x)}{\partial n_x} = \int_B M^{\mathrm{i}}(s,x)u(s)dB(s) - \int_B L^{\mathrm{i}}(s,x)\frac{\partial u(s)}{\partial n_s}dB(s), \quad x \in D \cup B, \tag{16}$$

and

$$0 = \int_B T^{\mathrm{e}}(s,x)u(s)dB(s) - \int_B U^{\mathrm{e}}(s,x)\frac{\partial u(s)}{\partial n_s}dB(s), \quad x \in D^c \cup B, \tag{17}$$

$$0 = \int_B M^{\mathrm{e}}(s,x)u(s)dB(s) - \int_B L^{\mathrm{e}}(s,x)\frac{\partial u(s)}{\partial n_s}dB(s), \quad x \in D^c \cup B. \tag{18}$$

For the exterior problem, the domain of interest is in the external region of the circular boundary and the complementary domain is in the internal region of the circle. Therefore, the null-field integral equations are represented as follows:

$$2\pi u(x) = \int_B T^{\mathrm{e}}(s,x)u(s)dB(s) - \int_B U^{\mathrm{e}}(s,x)\frac{\partial u(s)}{\partial n_s}dB(s), \quad x \in D \cup B, \tag{19}$$

$$2\pi \frac{\partial u(x)}{\partial n_x} = \int_B M^{\mathrm{e}}(s,x)u(s)dB(s) - \int_B L^{\mathrm{e}}(s,x)\frac{\partial u(s)}{\partial n_s}dB(s), \quad x \in D \cup B, \tag{20}$$

and

$$0 = \int_B T^{\mathrm{i}}(s,x)u(s)dB(s) - \int_B U^{\mathrm{i}}(s,x)\frac{\partial u(s)}{\partial n_s}dB(s), \quad x \in D^c \cup B, \tag{21}$$

$$0 = \int_B M^{\mathrm{i}}(s,x)u(s)dB(s) - \int_B L^{\mathrm{i}}(s,x)\frac{\partial u(s)}{\partial n_s}dB(s), \quad x \in D^c \cup B. \tag{22}$$

where the superscripts of "i" and "e" are selected interior and exterior degenerate kernels for fundamental solutions. The explicit forms of degenerate kernels will be elaborated later.

D. Expansions of the Fundamental Solution and Boundary Density

The closed-form fundamental solution as previously mentioned is

$$U(s,x) = \frac{-i\pi H_0^{(1)}(kr)}{2}, \tag{23}$$

where $r \equiv |s - x|$ is the distance between the source point and the field point, $H_0^{(1)}$ is the first-kind Hankel function of zeroth order, and $i^2 = -1$ is the imaginary number. To fully utilize the property of circular geometry, the mathematical tools, degenerate (separable or finite rank) kernel and Fourier series, are adopted for analytical calculation of boundary integrals.

Degenerate (Separable) Kernel for Fundamental Solutions. In the polar coordinates, the field point x and source point s can be expressed as (ρ, ϕ) and (R, θ), respectively. By using the addition theorem for separating the source point and field point, kernel functions, $U(s,x)$, $T(s,x)$, $L(s,x)$, and $M(s,x)$, are expanded in terms of degenerate kernel as shown below [12, 13]:

$$U(s,x) = \begin{cases} U^{\mathrm{i}}(s,x) = \dfrac{-i\pi}{2} \displaystyle\sum_{m=0}^{\infty} \varepsilon_m J_m(k\rho) H_m^{(1)}(kR) \cos[m(\theta - \phi)], & R \geq \rho, \\ U^{\mathrm{e}}(s,x) = \dfrac{-i\pi}{2} \displaystyle\sum_{m=0}^{\infty} \varepsilon_m J_m(kR) H_m^{(1)}(k\rho) \cos[m(\theta - \phi)], & R < \rho, \end{cases} \tag{24}$$

$$T(s,x) = \begin{cases} T^{\mathrm{i}}(s,x) = \dfrac{-\pi k i}{2} \displaystyle\sum_{m=0}^{\infty} \varepsilon_m J_m(k\rho) H_m'^{(1)}(kR) \cos[m(\theta - \phi)], & R > \rho, \\ T^{\mathrm{e}}(s,x) = \dfrac{-\pi k i}{2} \displaystyle\sum_{m=0}^{\infty} \varepsilon_m J_m'(kR) H_m^{(1)}(k\rho) \cos[m(\theta - \phi)], & R < \rho, \end{cases} \tag{25}$$

$$L(s,x) = \begin{cases} L^{\mathrm{i}}(s,x) = \dfrac{-\pi k i}{2} \displaystyle\sum_{m=0}^{\infty} \varepsilon_m J_m'(k\rho) H_m^{(1)}(kR) \cos[m(\theta - \phi)], & R > \rho, \\ L^{\mathrm{e}}(s,x) = \dfrac{-\pi k i}{2} \displaystyle\sum_{m=0}^{\infty} \varepsilon_m J_m(kR) H_m'^{(1)}(k\rho) \cos[m(\theta - \phi)], & R < \rho, \end{cases} \tag{26}$$

$$M(s,x) = \begin{cases} M^{\mathrm{i}}(s,x) = \dfrac{-\pi k^2 i}{2} \displaystyle\sum_{m=0}^{\infty} \varepsilon_m J_m'(k\rho) H_m'^{(1)}(kR) \cos[m(\theta - \phi)], & R \geq \rho, \\ M^{\mathrm{e}}(s,x) = \dfrac{-\pi k^2 i}{2} \displaystyle\sum_{m=0}^{\infty} \varepsilon_m J_m'(kR) H_m'^{(1)}(k\rho) \cos[m(\theta - \phi)], & R < \rho, \end{cases} \tag{27}$$

where superscripts "i" and "e" denote the interior and exterior cases for the expressions of kernel, respectively, and ε_m is the Neumann factor

$$\varepsilon_m = \begin{cases} 1, & m = 0, \\ 2, & m = 1, 2, \ldots, \infty. \end{cases} \tag{28}$$

It is noted that U and M kernels in Eqs. (24) and (27) contain the equal sign of $\rho = R$, whereas T and L kernels do not include the equal sign due to discontinuity. A simple figure for explaining the degenerate kernels in the interior problem is shown in Fig. 1(b).

Fourier Series Expansion for Boundary Densities. We apply the Fourier series expansion to approximate the boundary density and its normal derivative as expressed by

$$u(s) = a_0 + \sum_{n=1}^{\infty} (a_n \cos n\theta + b_n \sin n\theta), \quad s \in B, \tag{29}$$

$$\frac{\partial u(s)}{\partial n_s} = p_0 + \sum_{n=1}^{\infty} (p_n \cos n\theta + q_n \sin n\theta), \quad s \in B, \tag{30}$$

where a_n, b_n, p_n and q_n ($n = 0, 1, 2, \ldots$) are the Fourier coefficients and θ is the polar angle. For the Dirichlet (Neumann) problem, a_n and b_n are known (unknown), whereas p_n and q_n are unknown (known). In the real computation, the integrals can be analytically calculated by using the orthogonal property of Fourier series and the same number of terms (M) in Eqs. (24)–(27), (29), and (30) used in the summation instead of infinite terms. This method is one kind of semianalytical methods as errors only occur from the truncation of Fourier series.

E. Adaptive Observer System

To fully use the property of degenerate kernels for circular boundaries, an adaptive observer system is addressed as shown in Fig. 2. For the boundary integrals, the origin of the observer system can be adaptively located on the center of the corresponding boundary contour. The dummy variable in the circular boundary integration is the angle instead of radial coordinate R. By using the adaptive system, all the integrals can be easily calculated for multiple connected problems. F2

F. Linear Algebraic Equation

To calculate the Fourier coefficients, N ($N = 2M+1$) boundary nodes for each circular boundary are uniformly located on each circular boundary. From Eqs. (17) and (18) or Eqs. (21) and (22), we have

$$0 = \sum_{i=1}^{H} \int_{B_i} T(s,x)u(s)dB(s) - \sum_{i=1}^{H} \int_{B_i} U(s,x)\frac{\partial u(s)}{\partial n_s}dB(s), \quad x \in D^c \cup B, \tag{31}$$

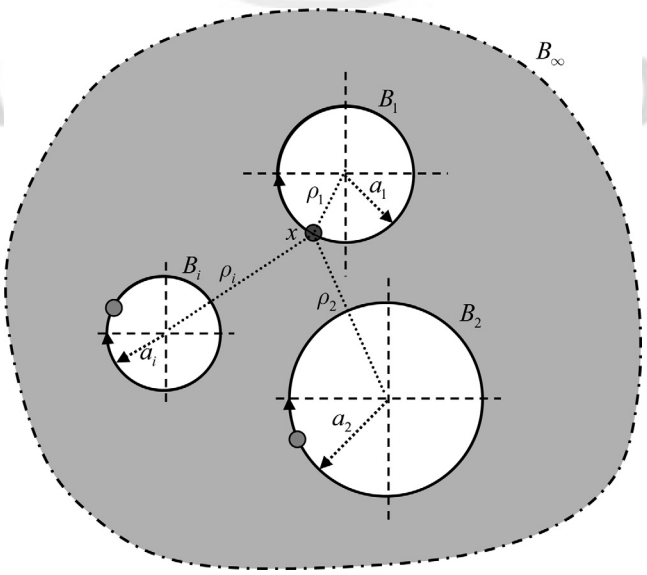

FIG. 2. Sketch of the null-field integral equation in conjuction with the adaptive observer system. [Color figure can be viewed in the online issue, which is available at www.interscience.wiley.com.]

$$0 = \sum_{i=1}^{H} \int_{B_i} M(s,x)u(s)dB(s) - \sum_{i=1}^{H} \int_{B_i} L(s,x)\frac{\partial u(s)}{\partial n_s}dB(s), \quad x \in D^c \cup B. \tag{32}$$

It is noted that the integration path is clockwise. For the integral of the circular boundary B_i, the kernels $[U(s,x), T(s,x), L(s,x)$, and $M(s,x)]$ are expressed by using the degenerate kernels and setting the origin at the center of B_i. The boundary densities $[u(s)$ and $\frac{\partial u(s)}{\partial n_s}]$ are substituted by using the Fourier series. The boundary contour integration can be analytically determined by the orthogonal relations of the Fourier base and the adaptive coordinate. The $2M+1$ boundary nodes are collocation points for satisfying BCs, instead of discretization for integrals. A linear algebraic system yields

$$[U]\{t\} = [T]\{u\}, \tag{33}$$

where $[U]$ and $[T]$ are the influence matrices with a dimension of $H \times (2M+1)$ by $H \times (2M+1)$, $\{u\}$ and $\{t\}$ denote the column vectors of Fourier coefficients with a dimension of $H \times (2M+1)$ by 1 for u and $\frac{\partial u}{\partial n}$, respectively. Only $2M+1$ unknown coefficients are sought for each circular hole, which can be determined by Eq. (33). Then, all the unknown boundary data can be determined and the potential is obtained by substituting the boundary data into Eq. (15) or (19). Based on the null-field integral equation approach, successful applications to Laplace [10, 20], Helmholtz [12, 13], biharmonic [21], and bi-Helmholtz [22] problems have been done.

III. METHODS OF SOLUTION

A. Problem Statements

The problem that we would like to study is the scattering problem with multiple cylinders arising from a point source, as shown in Fig. 3. The problem is governed by the Helmholtz operator as follows:

F3

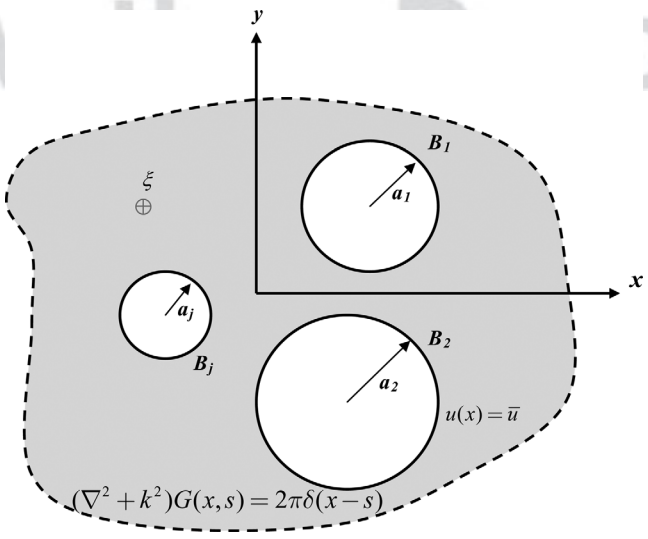

FIG. 3. Infinite plane with arbitrary number of circular cylinders subject to a point sound source at ξ. [Color figure can be viewed in the online issue, which is available at www.interscience.wiley.com.]

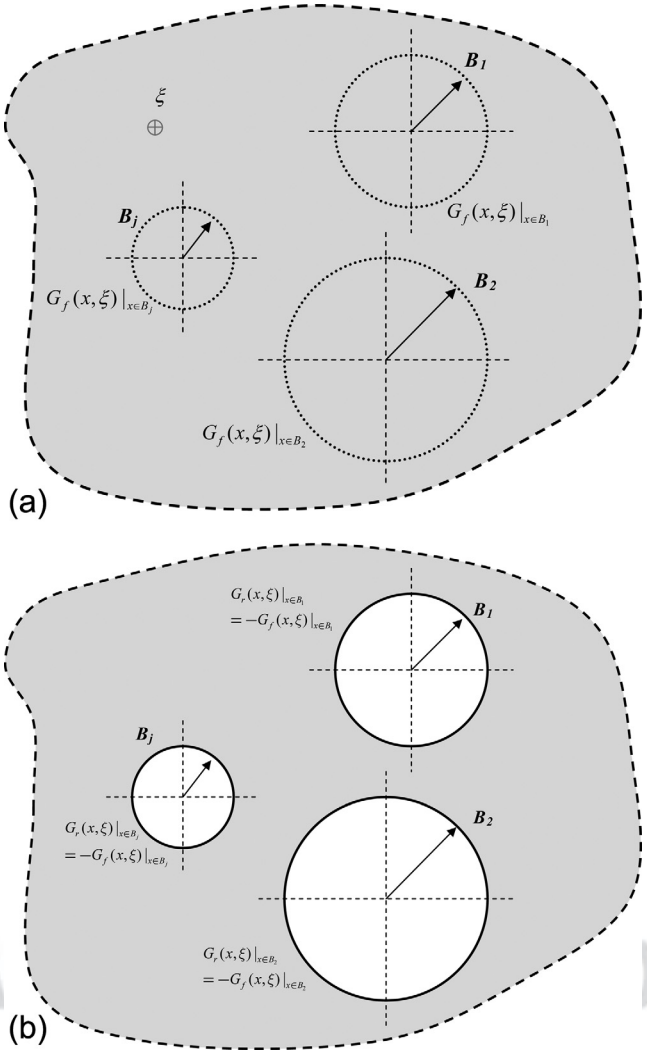

FIG. 4. (a) Free field of the fundamental solution. (b) Radiation field (a typical BVP). [Color figure can be viewed in the online issue, which is available at www.interscience.wiley.com.]

$$(\nabla^2 + k^2)G(x,\xi) = 2\pi\delta(x-\xi), \quad x \in D, \tag{34}$$

and the domain is bounded by

$$B = \bigcup_{j=1}^{H} B_j. \tag{35}$$

For acoustic wave, the soft boundary means the Dirichlet BC, whereas the hard boundary denotes the Neumann BC. Here, the cylinders are specified to soft boundaries as follows:

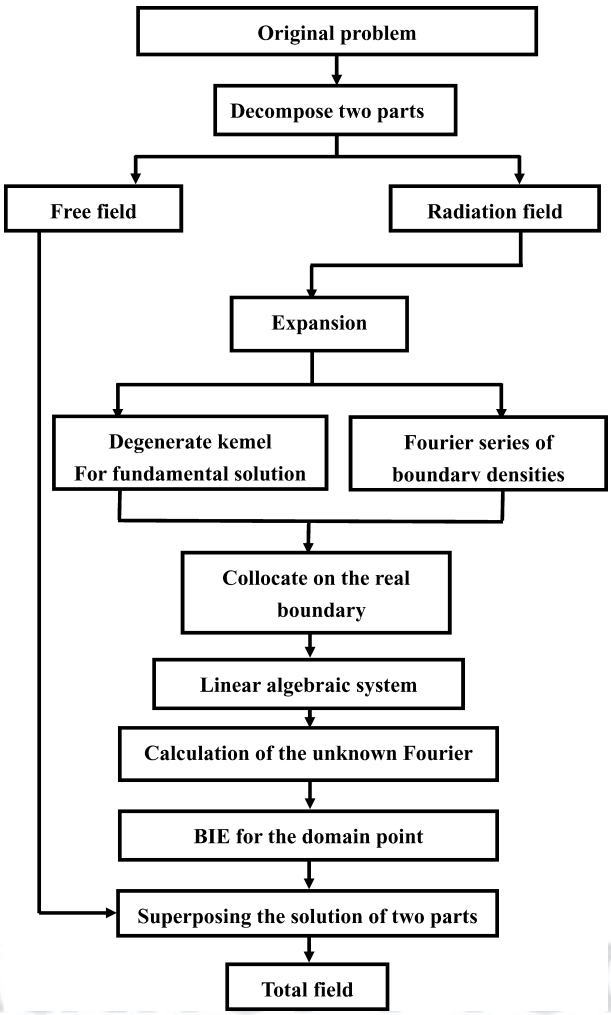

FIG. 5. Flowchart of the present approach.

$$G(x,\xi) = 0, \quad x \in B. \tag{36}$$

The proposed approach for solving the problem will be elaborated on the next section.

B. Green's Function Using the Addition Theorem and Superposition Technique

The scattering problem subject to a point sound source is shown in Fig. 3. It can be decomposed into two parts, the fundamental solution (free field) and the radiation field, as shown in Fig. 4(a,b). Based on the addition theorem, the fundamental solution can be separated into the series form using Eq. (24). For matching the boundary condition, the superposition of the artificial boundary condition $[G_f(x,\xi)]$ in Fig. 4(a) and the radiation boundary condition $[G_r(x,\xi)]$ in Fig. 4(b) must satisfy the original boundary condition in Fig. 3. The second part (radiation field) is a typical BVP and can be easily solved by using the null-field integral equation approach as mentioned in Section 2. For clarity, the flowchart of our method is shown in Fig. 5.

C. Green's Third-Identity Approach

Based on the Green's third identity, with respect to two systems u and v, we have

$$\int_D u(x)\nabla^2 v(x)dD(x) = \int_B u(x)\frac{\partial v(x)}{\partial n}dB(x) - \int_D \nabla u(x)\nabla v(x)dD(x), \tag{37}$$

$$\int_D [u(x)\nabla^2 v(x)dD(x) - v(x)\nabla^2 u(x)dD(x)] = \int_B [u(x)\frac{\partial v(x)}{\partial n} - v(x)\frac{\partial u(x)}{\partial n}]dB(x). \tag{38}$$

By selecting the fundamental solution $U(x,s)$ as u and the Green's function $G(s,\xi)$ as v, the Green's third identity gives

$$2\pi G(x,\xi) = \int_B T(s,x)G(s,\xi)dB(s) - \int_B U(s,x)\frac{\partial G(s,\xi)}{\partial n_s}dB(s) + U(\xi,x), \quad x \in D. \tag{39}$$

D. Equivalence Between the Solution Using the Green's Third Identity and Superposition Technique

The boundary integral equation for the free field problem can be written as follows:

$$2\pi G_f(x,\xi) = \int_B T(s,x)G_f(s,\xi)dB(s) - \int_B U(s,x)\frac{\partial G_f(s,\xi)}{\partial n_s}dB(s) + U(\xi,x), \quad x \in D, \tag{40}$$

where $G_f(x,\xi)$ is the free field. The boundary integral equation for the typical boundary value problem can be written as follows:

$$2\pi G_r(x,\xi) = \int_B T(s,x)G_r(s,\xi)dB(s) - \int_B U(s,x)\frac{\partial G_r(s,\xi)}{\partial n_s}dB(s), \quad x \in D, \tag{41}$$

where $G_r(x,\xi)$ is the second part solution for the typical BVP. By superimposing G_f and G_r in Eqs. (40) and (41), respectively, we have

$$2\pi[G_f(s,\xi) + G_r(s,\xi)] = \int_B T(s,x)[G_f(s,\xi) + G_r(s,\xi)]dB(s) - \int_B U(s,x)\left[\frac{\partial G_f(s,\xi)}{\partial n_s} + \frac{\partial G_r(s,\xi)}{\partial n_s}\right]dB(s) + U(\xi,x), \quad x \in D, \tag{42}$$

where $G_f(s,\xi) + G_r(s,\xi)$ and $\frac{\partial G_f(s,\xi)}{\partial n_s} + \frac{\partial G_r(s,\xi)}{\partial n_s}$ satisfy the original boundary conditions. By comparing Eq. (42) with Eq. (39), we can find $G(x,\xi) = G_f(x,\xi) + G_r(x,\xi)$. Therefore, we have proven the mathematical equivalence between the solution of Green's third identity and that of superposition technique.

IV. AN ILLUSTRATIVE EXAMPLE

We consider an infinite plane with two identical circular cylinders subject to a point sound source as shown in Fig. 6. The radii of the two identical cylinders are a. The locations of source and probe are at $(-100, 0)$ and $(2\lambda, y)$, respectively, where λ is the wave length. The distance between **F6**

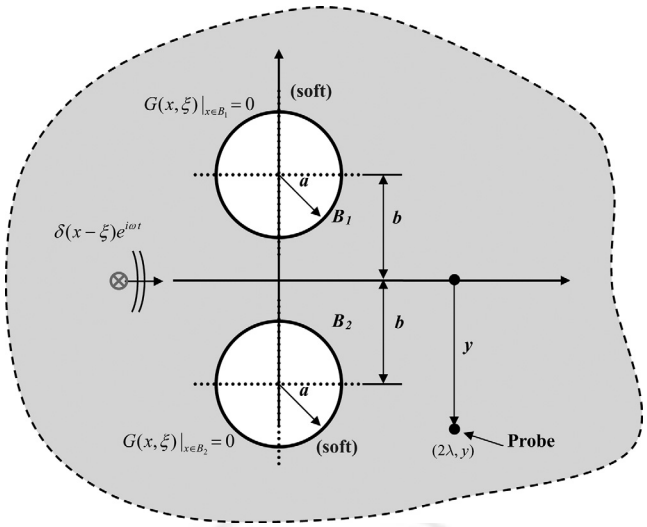

FIG. 6. An infinite plane with two equal circular cylinders subject to a point sound source. [Color figure can be viewed in the online issue, which is available at www.interscience.wiley.com.]

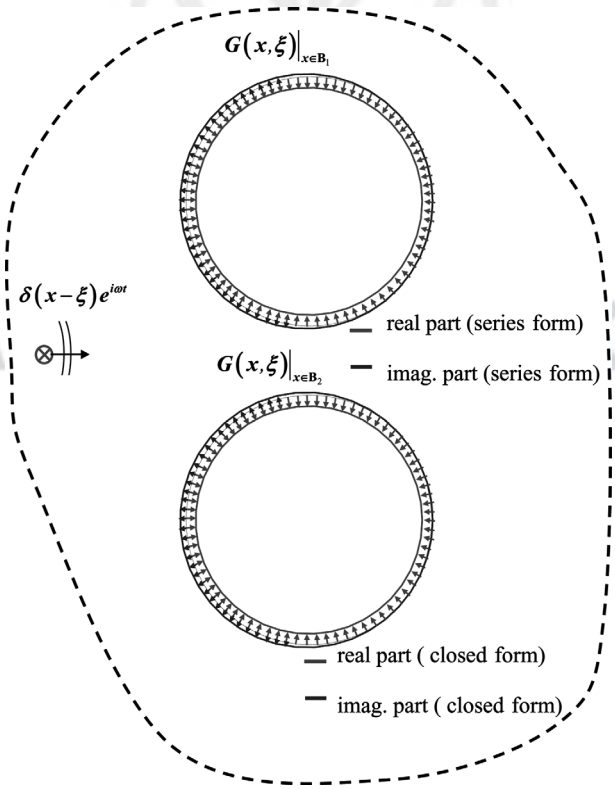

FIG. 7. Distribution potential on the artificial boundaries in the free field (upper part: series form; lower part: closed form, $M = 20$). [Color figure can be viewed in the online issue, which is available at www.interscience.wiley.com.]

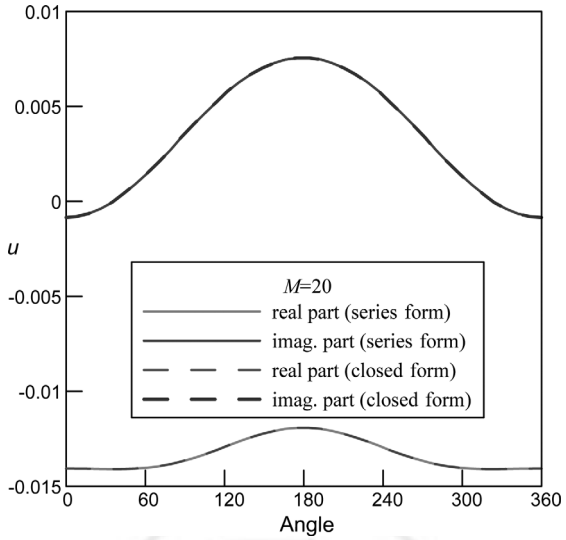

FIG. 8. Distribution potential on the artificial boundaries in the free field versus polar angle. [Color figure can be viewed in the online issue, which is available at www.interscience.wiley.com.]

the two centers of identical cylinders is $2b$. The boundary conditions are the Dirichlet types $[G(x,\xi) = 0]$ due to the soft cylinders. The potential distribution along the artificial boundary for the free field is shown in Figs. 7 and 8 versus circular boundary and polar angle, respectively. Both the closed-form formula of Eq. (23) and series-form formula of Eq. (24) are given. After obtaining the total field at the probe, the relative amplitude is defined by dividing the total field

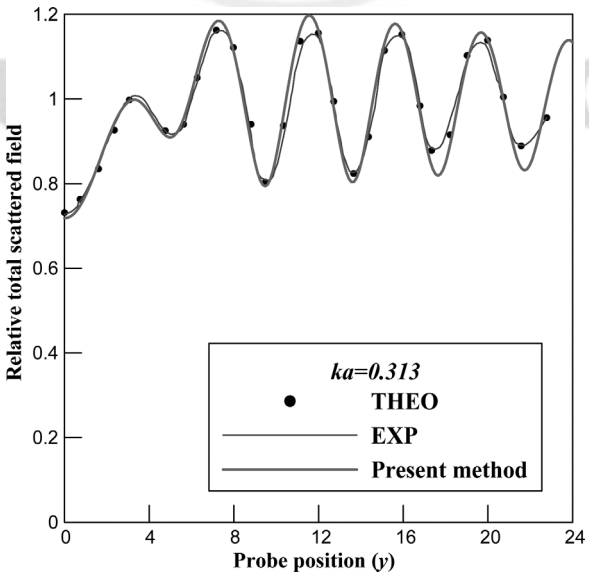

FIG. 9. Relative amplitude of total field versus the probe location y ($M = 20$). [Color figure can be viewed in the online issue, which is available at www.interscience.wiley.com.]

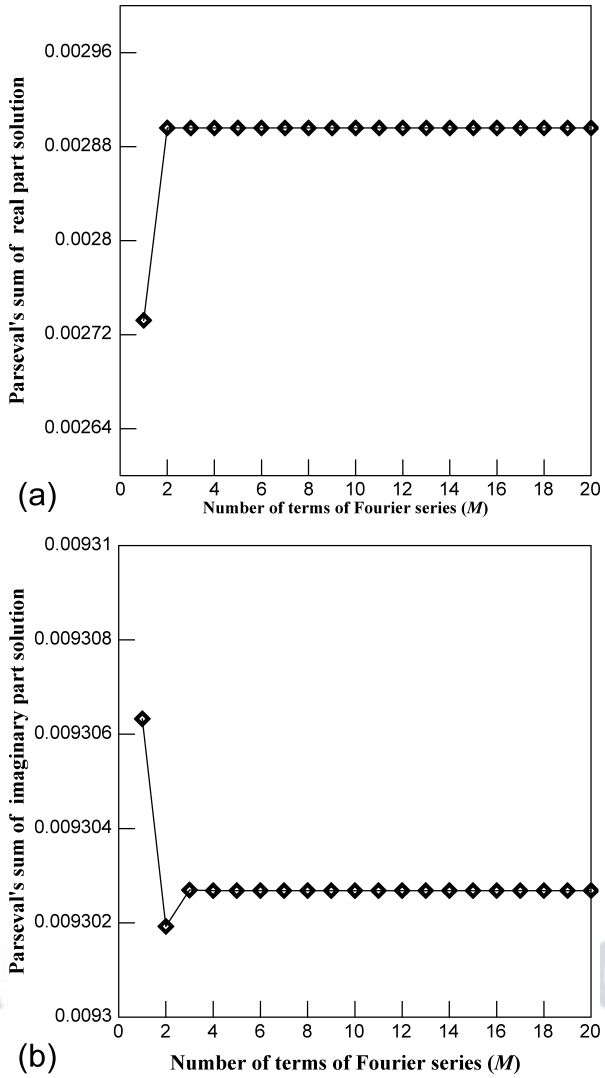

FIG. 10. Convergence test of Parseval's sum for (a) $\partial G(x,\xi)/\partial n_x$ (real part) and (b) $\partial G(x,\xi)/\partial n_x$ (imaginary part).

with respect to the free field at $(x, 0)$. By considering $\lambda = \pi$, $b = \frac{1}{2}\pi$, and $a = 0.05\lambda$, the relative
F9 amplitude of the total field versus y of probe location is shown in Fig. 9. The result agrees well with theoretical results and experimental data by Row [3]. The convergence rate is examined
F10 by using the Parseval's sum [18] in Fig. 10(a,b), for real and imaginary parts, respectively. The Parseval's sum is defined by

$$\int_0^{2\pi} \left(\frac{\partial u(s)}{\partial n_s}\right)^2 d\theta = 2\pi\, p_0^2 + \pi \sum_{n=1}^{M} \left(p_n^2 + q_n^2\right), \quad s \in B. \tag{43}$$

It is found that only few terms for Fourier series are required. In the real calculation, 20 terms are adopted. By changing the size of cylinder (a) and the same parameters of $\lambda = \pi$ and $b = \frac{1}{2}\pi$,

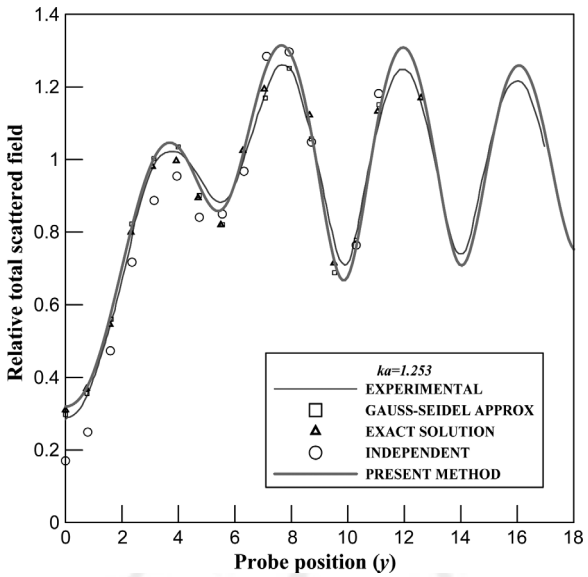

FIG. 11. Relative amplitude of total field versus the probe location ($M = 20$). [Color figure can be viewed in the online issue, which is available at www.interscience.wiley.com.]

AQ4

the relative amplitudes are shown in Figs. 11 and 12 for different sizes of cylinders $a = 0.2\lambda$ and $a = 0.318\lambda$, respectively. Agreement with the Row's data is observed. The approach is scheme stable as the linear algebraic equation is well posed by using the present approach. The diagonally dominant matrix is obtained as we exactly locate on the boundary point in the BIE. A condition number is in the $O(10^2)$. By setting the fixed probe at $(2\lambda, 0)$, the relative amplitudes versus

F11

F12

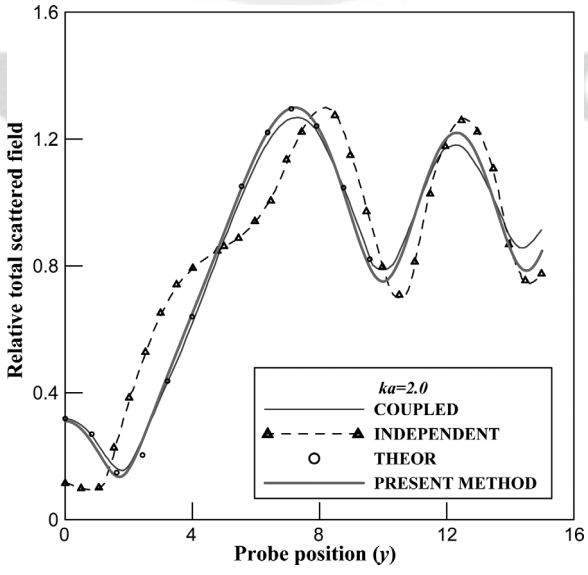

FIG. 12. Relative amplitude of total field versus the probe location ($M = 20$). [Color figure can be viewed in the online issue, which is available at www.interscience.wiley.com.]

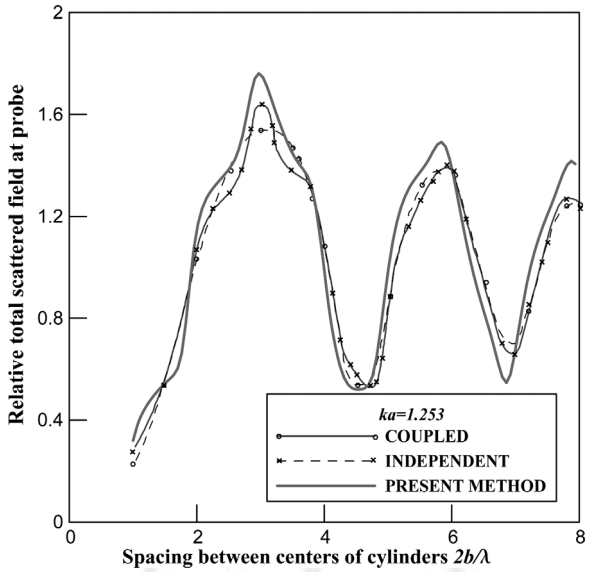

FIG. 13. Relative amplitude of total field versus $2b/\lambda$ ($a = 0.2\lambda$ and $M = 20$). [Color figure can be viewed in the online issue, which is available at www.interscience.wiley.com.]

the spacing between the two cylinders for $a = 0.2\lambda$, 0.24λ, 0.318λ, and 0.477λ are shown in
F13–16 Figs. 13–16, respectively, to see the effect of distance between the two cylinders for various sizes of cylinders. All the results in Figs. 13–16 agree well with the theoretical and experimental data by Row [3]. Although only two cylinders are considered in this proposed approach, our approach

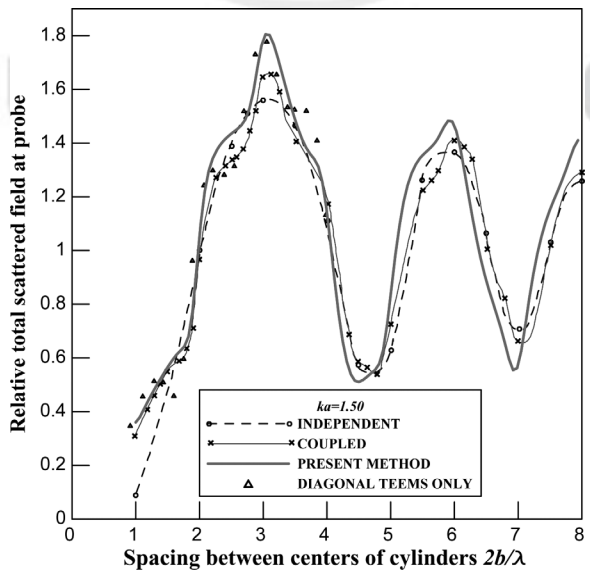

FIG. 14. Relative amplitude of total field versus $2b/\lambda$ ($a = 0.24\lambda$ and $M = 20$). [Color figure can be viewed in the online issue, which is available at www.interscience.wiley.com.]

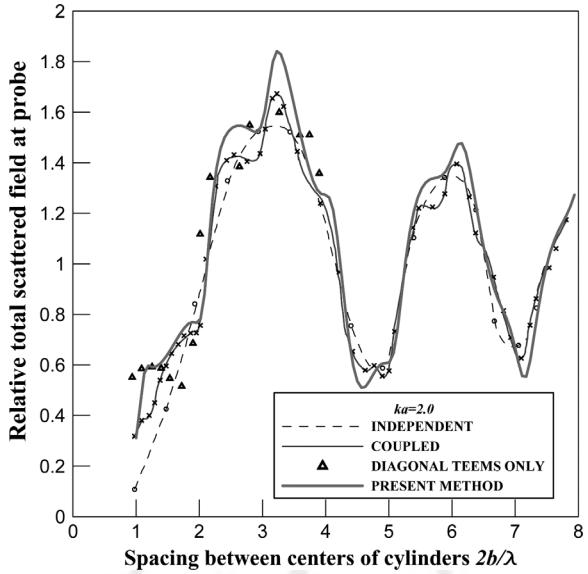

FIG. 15. Relative amplitude of total field versus $2b/\lambda$ ($a = 0.318\lambda$ and $M = 20$). [Color figure can be viewed in the online issue, which is available at www.interscience.wiley.com.]

can be extended to solve multiple cylinder problems without any difficulty. In this example, efficiency of the proposed method of the sound-scattering problem is verified. In addition, it can be extended to deal with scattering problem in different engineering areas, e.g., water-wave problem or electromagnetism, by following the same concept.

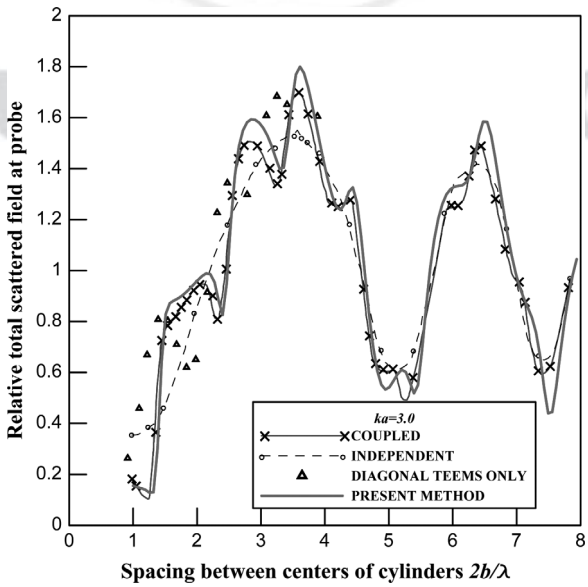

FIG. 16. Relative amplitude of total field versus $2b/\lambda$ ($a = 0.477\lambda$ and $M = 20$). [Color figure can be viewed in the online issue, which is available at www.interscience.wiley.com.]

V. CONCLUSIONS

In this article, we proposed the addition theorem and superposition technique to solve the scattering problem of two identical cylinders subject to a point source. Regarding the BVP with circular boundaries, we have proposed a BIEM formulation by using degenerate kernels, null-field integral equation, and Fourier series in companion with adaptive observer system. This method is a semianalytical approach for the problems with circular boundaries as only truncation error in the Fourier series is involved. A general-purpose program for solving the problems with arbitrary number, any size, and various locations of circular cylinders was developed. Therefore, not only the sound-scattering problems from a point source but also electromagnetic scattering problems can be solved by using this approach. Good agreement is observed after comparing with theoretical and experiment data.

References

1. S. E. Sherer, Scattering of sound from axisymmetric sources by multiple circular cylinders, J Acoust Soc Am 115 (2004), 488–496.
2. X. Antoine, C. Chniti, and K. Ramdani, On the numerical approximation of high-frequency acoustic multiple scattering problems by circular cylinders, J Comput Phys 227 (2008), 1754–1771.
3. R. V. Row, Theoretical and experimental study of electromagnetic scattering by two identical conducting cylinders, J Appl Phys 26 (1955), 666–675.
4. B. H. Henin, A. Z. Elsherbeni, and M. A. Sharkawy, Oblique incidence plane wave scattering from an array of circular dielectric cylinders, Prog Electromagn Res 68 (2007), 261–279.
5. Y. H. Pao, Elastic waves in solids, ASME J Appl Mech 50 (1983), 1152–1983.
6. C. M. Linton and D. V. Evans, The interaction of waves with arrays of vertical circular cylinders, J Fluid Mech 215 (1990), 549–569.
7. P. A. Martin, Multiple scattering—interaction of time-harmonic waves with N obstacles, Cambridge, New York, 2006.
8. R. V. Row, Microwave diffraction measurements in a parallel-plate region, J Appl Phys 24 (1953), 1448–1452.
9. H. A. Yousif and S. Köhler, Scattering by two penetrable cylinders at oblique incidence, J Opt Soc Am 5 (1988), 1085–1096.
10. J. T. Chen, W. C. Shen, and A. C. Wu, Null-field integral equations for stress field around circular holes under anti-plane shear, Eng Anal Bound Elem 30 (2006), 205–217.
11. J. T. Chen, C. T. Chen, and I. L. Chen, Null-field integral equation approach for eigenproblems with circular boundaries, J Comp Acoust 15 (2008), 1–28.
12. J. T. Chen, P. Y. Chen, and C. T. Chen, Surface motion of multiple alluvial valleys for incident plane SH-waves by using a semi-analytical approach, Soil Dyn Earthquake Eng 28 (2008), 58–72.
13. J. T. Chen, C. T. Chen, P. Y. Chen, and I. L. Chen, A semi-analytical approach for radiation and scattering problems with circular boundaries, Comput Methods Appl Mech Eng 196 (2008), 2751–2764.
14. Z. C. Li, Combined methods for elliptic problems with singularities, interfaces and infinities, Kluwer Academic Publishers, Boston, 1998.
15. Z. C. Li, Method of fundamental solutions for annular shaped domains, J Comput Appl Math 228 (2009), 355–372.
16. Z. C. Li, T. T. Lu, H. Y. Hu, and A. H. D. Cheng, Trefftz and collocation methods, WIT Press, Southampton, Boston, 2008.

17. T. W. Wu, Boundary element acoustics: fundamentals and computer codes, University of Kentucky, Kentucky, USA, 2000.

18. J. T. Chen and J. N. Ke, Derivation of anti-plane dynamic Green's function for several circular inclusions with imperfect interfaces, Comput Model Eng Sci 29 (2008), 111–135.

19. J. T. Chen, K. H. Chou, and S. K. Kao, Derivation of Green's function using addition theorem, Mech Res Commun 32 (2008), 108–121.

20. J. T. Chen and W. C. Shen, Null-field approach for Laplace problems with circular boundaries using degenerate kernels, Numer Methods Partial Differential Equations 25 (2009), 63–86.

21. J. T. Chen, W. M. Lee, and H. Z. Liao, Isotropic clamped-free thin annular circular plate subjected to a concentrated load, ASME J Appl Mech 75 (2008), 658–663.

22. W. M. Lee, J. T. Chen, and Y. T. Lee, Free vibration analysis of circular plates with multiple circular holes using indirect BIEMs, J Sound Vib 304 (2007), 811–830.